INTERNATIONAL JOURNAL OF

Applied Glass
SCIENCE

SPECIAL ISSUE ARTICLE

Structure and fluorescence properties of Dy-doped alkaline-earth borophosphate glasses

Kristin Griebenow[1] | Francisco Muñoz[2] | Nagia S. Tagiara[3] | Róbert Klement[1] | Anna Prnová[1] | Bruno Wolfrum[1] | Efstratios I. Kamitsos[3] | Alicia Duran[2] | Dušan Galusek[1,4]

[1]FunGlass, A. Dubček, University of Trenčín, Trenčín, Slovakia

[2]Institute of Ceramics and Glass (CSIC), Madrid, Spain

[3]Theoretical & Physical Chemistry Institute, National Hellenic Research Foundation, Athens, Greece

[4]VILA – Join Glass Centre of the IIC SAS, TnUAD, FChPT STU, Trenčín, Slovakia

Correspondence
Kristin Griebenow, FunGlass, A. Dubček University of Trenčín, Študentská 2, 911 50 Trenčín, Slovakia.
Email: kristin.griebenow@tnuni.sk

Abstract

Dysprosium-doped borophosphate glasses, containing the divalent cations Mg^{2+}, Ca^{2+}, Sr^{2+}, Ba^{2+}, and Zn^{2+}, are prepared by the melt-quenching technique. The structure of the glasses is investigated by Raman, infrared, and nuclear magnetic resonance (NMR) spectroscopies and the fluorescence properties are determined. The Dy^{3+} emission lifetime increases with an increasing ionic field strength and its maximum is observed in the Mg^{2+} and Zn^{2+} containing glasses. This result can be explained by the stronger M-O bonding which causes a rearrangement of the borophosphate network and creates a local Dy^{3+} environment of comparably low symmetry. This is in agreement with the Raman spectra and the evolution of the molar volume. The effect of the B/P variation on the emission properties of Dy^{3+} is investigated in a second series of glasses where the emission lifetime is found to be maximum at 10 mol% B_2O_3.

KEYWORDS
borophosphate glasses, dysprosium, far infrared spectroscopy, luminescence, Raman spectroscopy

1 | INTRODUCTION

The numerous applications of rare-earth (RE)-doped glasses in photonic and optophotonic devices have drawn much attention to these materials over the last decade and new materials have to be continuously developed. Important criteria for successful luminescent materials are a good optical performance, a long lifetime, and comparatively low production costs. Glasses doped with rare-earth ions have been intensively investigated for years to

find suitable candidates meeting these criteria. Due to their relatively sharp and intense emissions in the visible, near-infrared, and infrared spectral regions, several potential applications have been identified for RE-doped glasses such as solid-state lasers and lighting, optical amplifiers, color display devices, and optical sensors. It was shown that the emission properties of the RE ions strongly depend on the host matrix, the network modifiers and the doping concentration.[1] Among the RE ions Dy^{3+} is particularly interesting for white light generation applications as Dy^{3+} shows two major emission bands; one in the blue and another in the yellow part of the visible spectrum. Therefore, a white light emission can be generated by tuning and combining these two bands. Phosphate glasses are often used as the host matrix as they can incorporate comparatively high amounts of RE ions. Additional advantages are their good transparency, low melting point, and low dispersion, while a drawback of pure phosphate glasses is their sensitivity to water, that is, corrosion.

The phosphate glass network is composed of PO_4 tetrahedra which are connected through covalent phosphorous-oxygen bonds and are therefore able to form a polymerized structure whose degree of bonding depends on the glass composition.[2] The Q^i nomenclature is used to describe the phosphate glass structure, where i denotes the number of bridging oxygen atoms. Borate glasses instead are composed of trigonal BO_3 and tetrahedral BO_4 units, but their relative amounts strongly depend on the glass composition.[3] The effect of introducing B_2O_3 into the phosphate network is strongly dependent on the B/P ratio and the overall network former content.[4,5] Therefore, the glass structure of BP glasses can be adjusted to not only improve the emission properties of the dopant but also to enhance the chemical and thermal stability.[6,7] BP glasses containing divalent cations such as Ba^{2+}, Sr^{2+}, and Zn^{2+} have been investigated with respect to their structure as well as thermal and physical properties.[8–13] Several studies report the potential of BP glasses as a host matrix for RE ions like Dy^{3+}, Yb^{3+}, and Sm^{3+}.[14–20]

Karki et al. investigated the influence of the Dy_2O_3 doping concentration on the emission properties of a Ba^{2+} containing BP glass with the mol% composition $25BaO-5B_2O_3-(70-x)P_2O_5-xDy_2O_3$ with Dy_2O_3 concentrations between 0.2 and 1.0 mol%.[17] The color chromaticity coordinates of these glasses indicate their potential as white light-emitting materials. Jayasimhadri et al. performed a similar study for the glass composition $40ZnO-30B_2O_3-30P_2O_5$ (in mol%) adding up to 0.5 mol% Dy_2O_3 and the emission results also indicate the suitability for white light applications.[15] Chanthima et al. studied the influence of the network modifier on the emission properties of Dy^{3+} in the glasses $25Bi_2O_3-5B_2O_3-69P_2O_5-1Dy_2O_3$ and $25BaO-5B_2O_3-69P_2O_5-1Dy_2O_3$ (mol%), respectively.[16] They found a higher emission intensity in the Ba^{2+} containing BP glass.

The work presented here investigates the influence of the divalent cation species M^{2+}, that is, Mg^{2+}, Ca^{2+}, Sr^{2+}, Ba^{2+}, or Zn^{2+}, on the emission properties of Dy^{3+} in the first set of glasses with the mol% composition $40MO-10B_2O_3-50P_2O_5 + xDy_2O_3$ with $x = 0.0$, 0.1, or 0.3 mol%. The amounts of added Dy_2O_3 were chosen to test a luminescence range rather than to optimize this property. The influence of the B/P ratio on the emission of Dy^{3+} is studied in the second set of glasses $40ZnO-xB_2O_3-(60 - x)P_2O_5 + 0.1Dy_2O_3$ (mol%). A structural study of the BP glasses by combining Raman, Fourier-Transform Infrared (FTIR), and Magic Angle Spinning (MAS) Nuclear Magnetic Resonance (NMR) spectroscopy results is also presented.

2 | EXPERIMENTAL

2.1 | Glass series A

Glasses with the chemical compositions $40MO-10B_2O_3-50P_2O_5 + xDy_2O_3$ in mol% (with M = Mg, Ca, Sr, Ba, or Zn and $x = 0$, 0.1, or 0.3) were prepared by mixing appropriate amounts of the respective raw materials in batches of 50 g (H_3BO_3, $NH_4H_2PO_4$, $CaCO_3$, and ZnO from Centralchem with purities ≥99%, basic $MgCO_3$ and $BaCO_3$ from AFT Bratislava with a purity of 95% and ≥99%, $SrCO_3$ from Sigma-Aldrich (≥99.9%) and Dy_2O_3 (99.9%) from Treibacher Industrie AG). The powders were heated to temperatures of up to 1350°C (depending on glass composition) in alumina crucibles placed in a resistance-heated furnace. After 2 h, the melts were poured into preheated graphite molds and kept at temperatures ~20°C above their respective glass transition temperatures (T_g) for 30 min before cooling to room temperature.

2.2 | Glass series B

Glasses with the chemical compositions $40ZnO-xB_2O_3-(60-x)P_2O_5 + 0.1Dy_2O_3$ mol% ($x = 0$, 5, 15) were prepared as 50 g batches by mixing appropriate amounts of $NH_4H_2PO_4$ (Acros organics, 99%), ZnO (Panreac, 99%), B_2O_3, and Dy_2O_3 (Alfa Aesar, 99% and 99.99%). The powders were heated to 450°C in alumina crucibles and held for ≈10 h before the temperature was increased up to 1320°C, depending on the composition. The melts with $x = 0$ and 5 mol% B_2O_3 were poured into preheated graphite molds. To avoid crystallization, the melt with $x = 15$ mol% B_2O_3 was quenched between a brass plate and stamp. The glasses were transferred to a muffle furnace and kept for 30 minutes at ≈20°C above their respective T_g values before cooling to room temperature. All glasses were transparent and colorless, containing

TABLE 1 Sample names, corresponding nominal compositions in mol%, ρ (± 0.003 g/cm^3) and T$_g$ (± 3°C) of the studied glasses

Sample name	MgO	CaO	SrO	BaO	ZnO	Dy$_2$O$_3$	B$_2$O$_3$	P$_2$O$_5$	ρ [g/cm^3]	T$_g$ [°C]
MgBP	40					0	10	50	2.383	614
MgBP_01	40					0.1	10	50	2.436	617
MgBP_03	40					0.3	10	50	2.415	620
CaBP		40				0	10	50	2.613	593
CaBP_01		40				0.1	10	50	2.628	597
CaBP_03		40				0.3	10	50	2.639	601
SrBP			40			0	10	50	3.054	578
SrBP_01			40			0.1	10	50	3.131	585
SrBP_03			40			0.3	10	50	3.036	583
BaBP				40		0	10	50	3.302	544
BaBP_01				40		0.1	10	50	3.388	555
BaBP_03				40		0.3	10	50	3.389	559
ZnBP					40	0	10	50	2.799	532
ZnBP_01					40	0.1	10	50	2.787	536
ZnBP_03					40	0.3	10	50	2.769	539
ZnP_01					40	0.1	0	60	2.808	430
Zn5B55P_01					40	0.1	5	55	2.732	462
Zn15B45P_01					40	0.1	15	45	2.849	530

only a few bubbles. An overview of the nominal compositions of the prepared glasses and the sample names is given in Table 1.

The glass density was measured in a Helium pycnometer Quantachrome Ultrapyc 1200e with a cell of 10 cm^3 using bulk samples. The glass samples were kept at 23°C before the density measurement. The samples were weighed using an analytical balance OHAUS Explorer EX125D00 scale with an accuracy ±0.0001 g.

The glass transition temperatures were determined through differential scanning calorimetry (DSC). DSC measurements were performed from 35 to 1000°C in nitrogen atmosphere using a heating rate of 10°C/min and a Netzsch STA 449 F1 Jupiter simultaneous thermal analyzer.

Infrared spectra were collected on a Fourier transform vacuum spectrometer in the reflectance mode (Vertex 80v, Bruker), in the range 30–7000 cm^{-1} with a resolution of 2 cm^{-1}. The reflectance spectra were analyzed by Kramers–Kronig transformation to calculate the real and imaginary parts of the complex refractive index, and the absorption coefficient spectra $\alpha(\nu)$ were obtained from the expression:

$$\alpha(v) = 4\pi v k(v), \tag{1}$$

where $k(\nu)$ is the imaginary part of the complex refractive index and ν is the infrared frequency in wavenumbers, cm^{-1}.[21]

The Raman spectra were recorded with 633 nm excitation in the range 200–1500 cm^{-1} with a Renishaw Raman Microscope inVia. Reflex, using the 20x objective and 10 s exposure time.

Magic Angle Spinning Nuclear Magnetic Resonance (MAS-NMR) measurements were performed using a Bruker AV-400-WB spectrometer, at the ^{31}P NMR frequency of 161.9 MHz and the ^{11}B NMR frequency of 128.37 MHz. A triple-resonance MAS probe supporting rotor was used with an outer diameter of 4 mm and a spinning speed of up to 10 kHz for both nuclei. ^{31}P MAS NMR spectra were acquired with a π/2 single pulse at 60 kHz, a spectral width of 100 kHz and a relaxation time of 40 s during 128 scans. All measurements were performed at room temperature, using H$_2$PO$_4$(NH$_4$) as a secondary external reference at 0.81 ppm relative to H$_3$PO$_4$ (85%) as the primary reference. ^{11}B MAS NMR spectra were acquired in a single pulse experiment with a π/15 pulse at 95 kHz, 100 kHz of spectral width during 1024 scans, and a 3 s relaxation delay. BF$_3$·Et$_2$O was used as a reference.

The photoluminescence excitation (PLE) and emission spectra (PL) were recorded at room temperature using a Fluorolog FL3-21 spectrometer (Horiba, France) in the front-face configuration. The Xe-lamp (450 W) was used as an excitation light source. The appropriate cut-off filters were used to eliminate the higher-order reflection artifacts in the PL spectra. The emission spectra were recorded at the same conditions (slit width, integration time, excitation/monitored wavelength) and corrected for the spectrometer optics and the excitation lamp response; while the PLE spectra were only corrected for the spectrometer optics.

The luminescence decay curves were recorded at room temperature with the same instrument at two monitored emission wavelengths corresponding to the blue (480 nm) and

yellow (572 nm) emission, using an excitation wavelength of 348 nm. The flash Xe-lamp was used as an excitation source. The decay curves were normalized and fitted using a double-exponential function.

3 | RESULTS

3.1 | Glass series A: 40MO-10B$_2$O$_3$-50P$_2$O$_5$ + xDy$_2$O$_3$ mol%, M = Mg^{2+}, Ca^{2+}, Sr^{2+}, Ba^{2+} or Zn^2, x = 0, 0.1, 0.3

3.1.1 | Glass properties

Figure 1 presents the glass transition temperatures and the densities of the undoped glasses with the general composition 40MO-10B$_2$O$_3$-50P$_2$O$_5$ as a function of the respective cation field strength at the oxygen ion.[22] An average ionic field strength of 0.49 A^{-2} was taken for Mg^{2+}, as both coordination sites (four and sixfold) were reported earlier in, for example, metaphosphate glasses.[23] The T$_g$ of the alkaline-earth (AE)-containing glasses increases nonlinearly from 544°C (Ba^{2+}) to 614°C (Mg^{2+}), whereas the Zn^{2+} containing glass has the lowest T$_g$ (532°C). The density of the glasses shows the opposite trend and decreases from Ba^{2+} (3.302 g/cm^3) to Mg^{2+} (2.383 g/cm^3), whereas the Zn^{2+} containing glass has a density of 2.799 g/cm^3. All density and T$_g$ values are reported in Table 1: introducing up to 0.3 mol% Dy$_2$O$_3$ leads to a minor increase in both the density (+ 0.08 g/cm^3) and T$_g$ (+ 8°C). It is noteworthy that the actual chemical compositions of the glasses were not analyzed. As the glasses in this study were melted in alumina crucibles, it is expected from previous investigations that up to a maximum of 3 mol% Al$_2$O$_3$ may be dissolved in the glass.[24] Other studies showed that crucible material and raw material have a significant influence on the glass properties.[25,26]
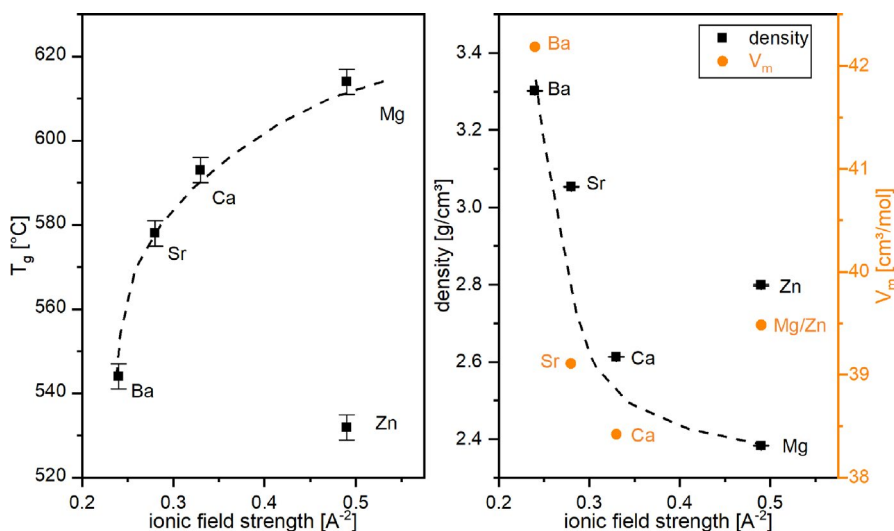
3.1.2 | Structural analysis

The Raman spectra of the BP glasses with varying divalent cations are presented in Figure 2. The most intense band, peaking between 1204 and 1155 cm^{-1}, corresponds to the symmetric stretching vibration of the terminal PO$_2^-$ units of Q^2 phosphate groups (ν_s(PO$_2$)). The broad feature between 1250 and 1400 cm^{-1} combines contributions from the asymmetric stretching vibration of the terminal PO$_2^-$ units in Q^2 groups (ν_{as}(PO$_2$)) and the symmetric stretching vibration of
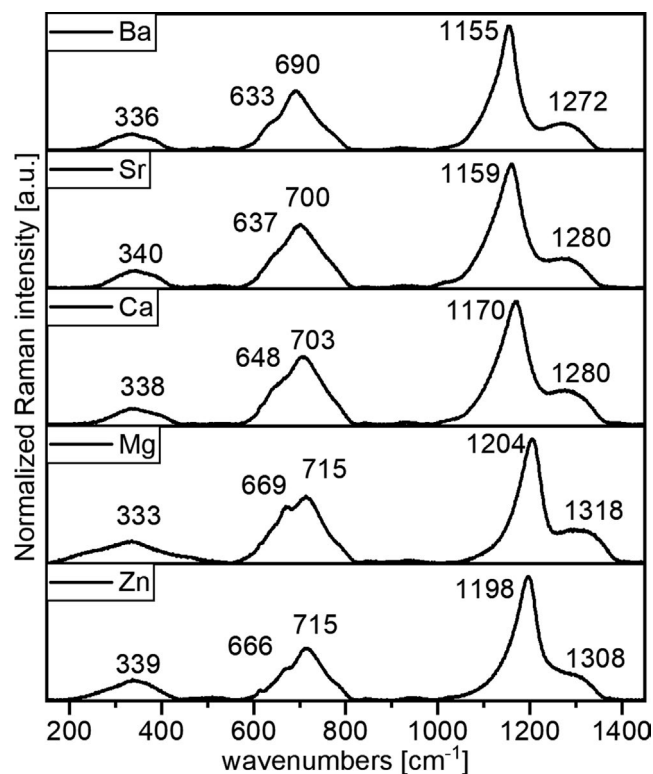

FIGURE 2 Normalized Raman spectra of the undoped glass series A recorded at 633 nm

FIGURE 1 Left: Glass transition temperatures of the undoped glass series A as a function of the field strength of the cation. Right: Density (black) and molar volume (orange) of the same glass compositions as a function of the cation field strength. If not discernible, the error margin is within the symbol size. The lines are drawn to guide the eye

P=O in phosphate Q^3 units.[25,27] The broad feature between 600 and 800 cm^{-1} can be assigned to the symmetric stretching vibrations of P-O-B units[4] and the breathing of borophosphate rings.[8] The minor feature at ≈ 337 cm^{-1} is due to the bending vibrations of the phosphate network.[8] All bands shift to lower wavenumbers when heavier alkaline-earth ions are present. The width of the most intense band ($\nu_s(PO_2)$) follows the order Ca^{2+} (81 cm^{-1}), Sr^{2+} (72 cm^{-1}), Zn^{2+}/Mg^{2+} (64 and 62 cm^{-1}), and Ba^{2+} (54 cm^{-1}). The Mg^{2+} containing glass shows a pronounced shoulder at ≈ 669 cm^{-1} on the broad feature between 600 and 800 cm^{-1} relative to the other glasses.

The Raman and calculated absorption coefficient spectra of the glass with the composition $40ZnO-10B_2O_3-50P_2O_5$ are presented in Figure 3. The absorption coefficient spectrum can be separated into three main regions: in the far-infrared (<500 cm^{-1}) the cation-oxygen motion is observed: $\nu(Zn-O) \approx 220$ and 280 cm^{-1}. Between 400 and 800 cm^{-1} two features occur and can be attributed to bending vibrations of the phosphate network ($\delta(P-O) = 425-640$ cm^{-1}) and to the symmetric stretching vibrations of P-O-P bridges, $\nu_s(P-O-P) \approx 680-820$ cm^{-1}. The third region between 800 and 1400 cm^{-1} is dominated by a broad feature with several peaks. It can be attributed to the asymmetric stretching vibrations of P-O-P in chain or ring formations (980 cm^{-1}), the asymmetric stretching of PO_3^{2-} groups in Q^1 units

($\nu_{as}(PO_3^{2-}) = 1100$ cm^{-1}), and the asymmetric stretching of Q^2 and Q^3 units ($\nu_{as}(Q^2)+\nu_{as}(Q^3) \approx 1250$ cm^{-1}). The region from 800 to 1150 cm^{-1} should also contain the contribution of B-O stretching modes of BO_4 tetrahedral units,[21,28] however, they overlap with the activity of the phosphate network.

The calculated absorption coefficient spectra of the glasses with varying metal cations are presented in Figure 4. Major differences are seen in the far-infrared region due to the presence of the cation-oxygen motion bands with $\nu(Ba-O) \approx 140$ cm^{-1}, $\nu(Sr-O) \approx 175$ cm^{-1}, $\nu(Ca-O) \approx 260$ cm^{-1}, $\nu(Zn-O) \approx 220$ and 280 cm^{-1}, and $\nu(Mg-O) \approx 400$ cm^{-1}, in agreement with previous studies in alkaline-earth metaphosphate glasses.[23,24,27] Differences are also observed in the region between 800 and 1400 cm^{-1}, which result from the convolution of the asymmetric stretching vibrations of P-O-P bridges, and of Q^1, Q^2, and Q^3 units. It is worth noting that the band attributed to the asymmetric stretching of Q^2 and Q^3 units appears at the highest frequency for the Mg^{2+} (1298 cm^{-1}) and Ba^{2+} (1281 cm^{-1}) containing glasses. As mentioned above, the B-O stretching modes of BO_4 tetrahedral units overlap with the phosphate activity in the 800-1150 cm^{-1} region. Therefore, a detailed spectral deconvolution would be necessary to correlate with the corresponding NMR results and make trustworthy band assignments. In any case, the absence of absorption bands above 1300 cm^{-1} in Figure 4 suggests the absence of three-fold coordinated
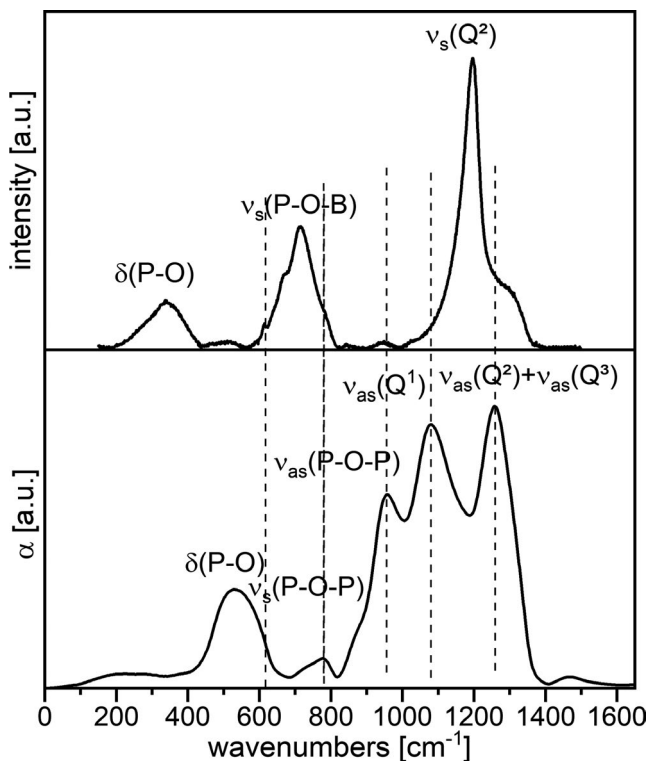

FIGURE 3 Raman (top) and calculated absorption coefficient spectra (bottom) of the glass with the composition $40ZnO-10B_2O_3-50P_2O_5$
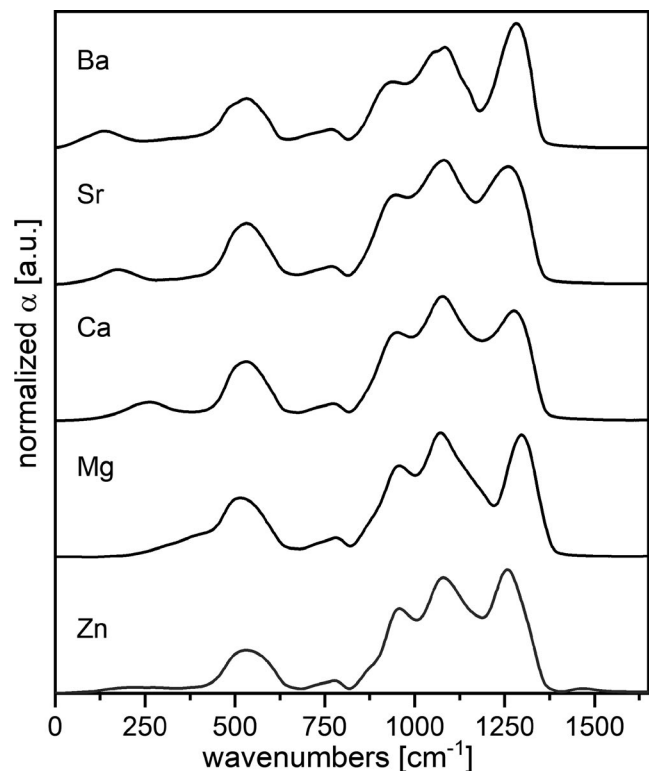

FIGURE 4 Calculated absorption coefficient spectra of the glasses with the compositions $40MO-10B_2O_3-50P_2O_5$
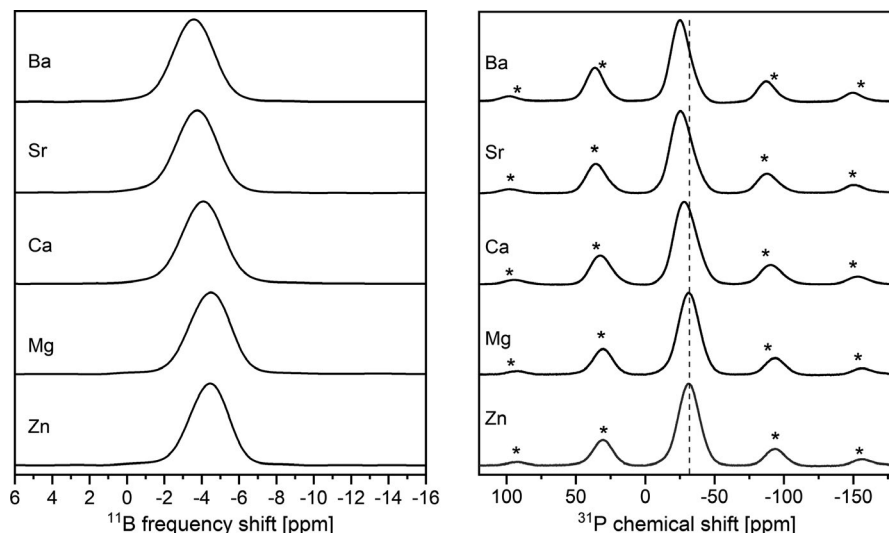
FIGURE 5 Left: ^{11}B MAS-NMR spectra of the glasses with the nominal compositions $40MO-10B_2O_3-50P_2O_5$ mol%. Right: corresponding ^{31}P MAS-NMR spectra. All spectra are normalized to their most intense peak
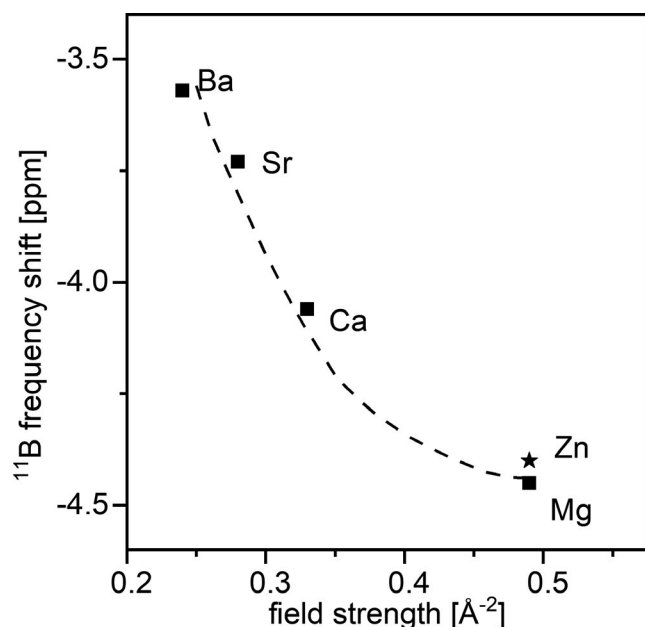

FIGURE 6 ^{11}B frequency shift of the undoped glass series A as a function of the field strength of the respective cation. The line is drawn to guide the eye

boron sites in the studied glasses. In low-alkali borosilicate glasses, for example, the B-O stretching is observed at 1370–1390 cm^{-1} for BO_3 sites and at 920–930 cm^{-1} for BO_4 sites.[29]

The ^{11}B and ^{31}P MAS-NMR spectra of the undoped glasses with 10 mol% B_2O_3 are presented in Figure 5. The ^{11}B spectra (Figure 5 left) show one broad resonance between 0 and −8 ppm which is the region of B in the tetrahedral configuration with 4 oxygen atoms (BO_4). The spectra were further analyzed using the *dmfit* software, release 20200306,[30] and could be simulated with a single Gaussian band. As shown in Figure 6, the band position shifts to higher fields as the cation field strength increases: Ba^{2+}(−3.6 ppm), Sr^{2+}(−3.7 ppm), Ca^{2+}(−4.1 ppm), Zn^{2+}(−4.4 ppm), and Mg^{2+}(−4.5 ppm).

Therefore, NMR spectroscopy confirms the presence of BO_4 sites and the absence of BO_3 sites in agreement with the results of infrared spectroscopy.

The ^{31}P spectra (Figure 5 right) show one signal between −20 and −50 ppm which shifts to higher fields with an increasing cation field strength. The spectra were further analyzed with the *dmfit* software.[30] The simulation of the spectra revealed at least two possible ^{31}P species, in agreement with Raman and infrared spectroscopy. The majority of P forms Q^2-type groups with a signal between −25 ppm (Ba^{2+}) and −34 ppm (Mg^{2+}). The remaining P form Q^3 groups with a signal between −38 ppm (Ba^{2+}) and −45 ppm (Mg^{2+}). Both signals shift to more negative ppm as the cation field strength increases (see Figure 7 top). This trend is almost linear for the AE-containing glasses, whereas the Zn^{2+} containing glass fall out of this trend. The relative amount of Q^3 groups also increases with the cation field strength but has a pronounced maximum in the Zn^{2+} glass composition (see Figure 7 bottom). Although the simulation of the ^{31}P MAS NMR spectra with two bands leads to simple results, there are most probably more species present as the formation of P–O–B bonds is expected. The signals of these species would also appear in the spectral region of the Q^2 and Q^3 bands. A recent study on Zn^{2+} containing borophosphate glasses reported a rather complex phosphate speciation.[31] Therefore, the presented results of the simulated ^{31}P NMR spectra have limited value.

3.1.3 | Optical and luminescence spectra

The optical absorption and excitation spectra of the glasses doped with 0.3 mol% Dy_2O_3 are presented in Figure 8. The absorption spectra show 12 transitions originating from the ground state $^6H_{15/2}$ to different excited states of the Dy^{3+} ions, with six broad bands between 740 and 1750 nm and sharper bands being present below 500 nm. The absorption spectra
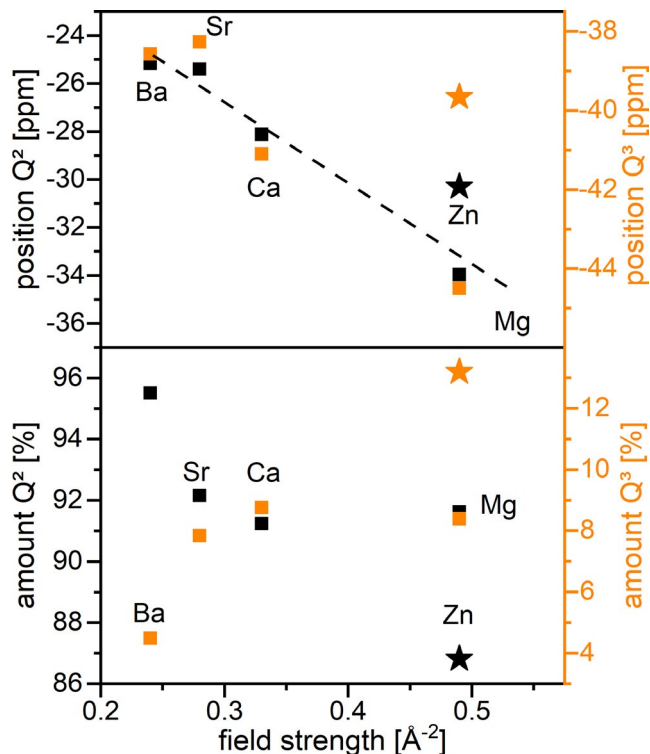
FIGURE 7 Q^2 (black) and Q^3 (orange) chemical shifts at the top and their total amounts at the bottom obtained from the deconvolution of the ^{31}P MAS-NMR spectra as a function of the cation field strength
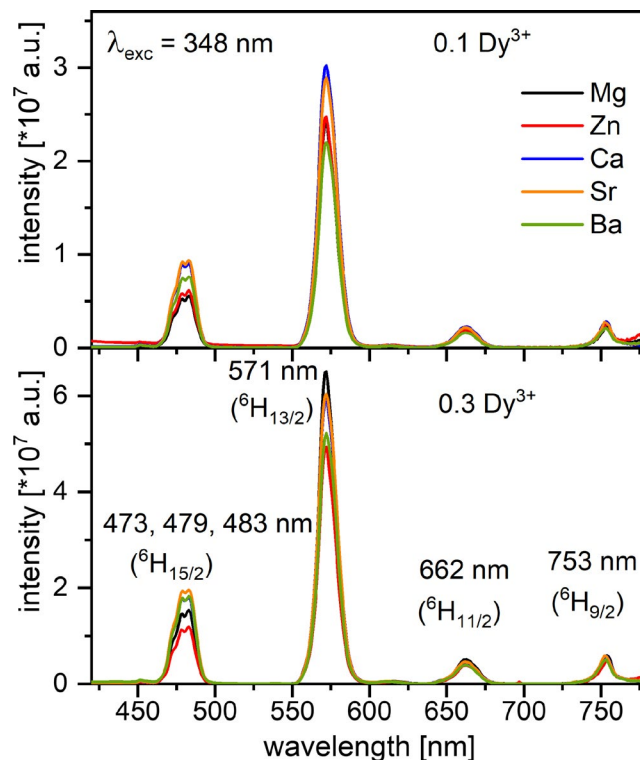

FIGURE 9 Emission spectra of the glass series A doped with 0.1 (top) and 0.3 (bottom) mol% Dy_2O_3 under an excitation of 348 nm
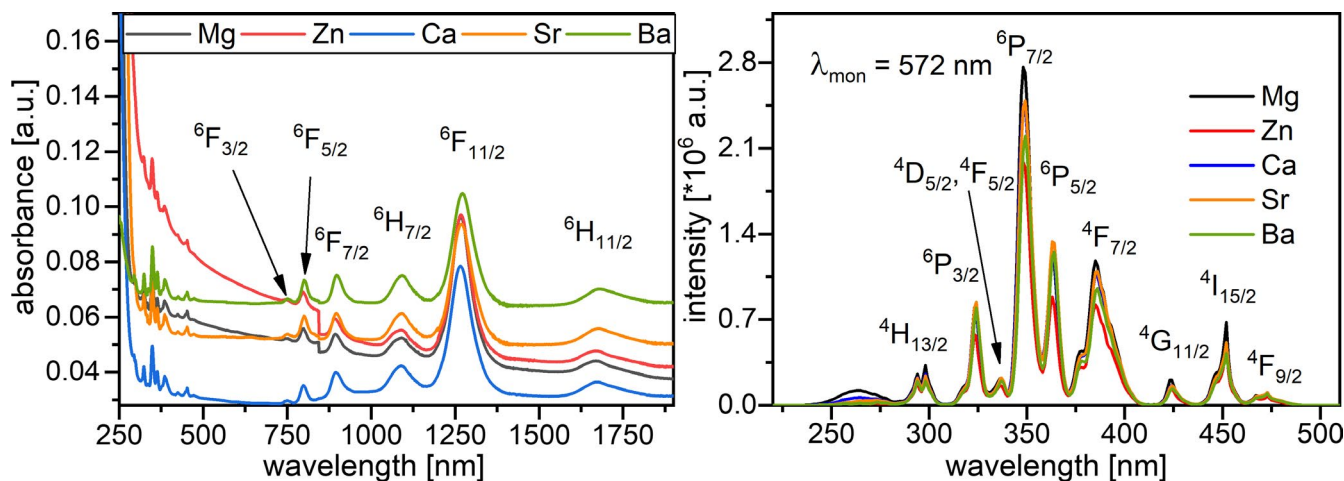

FIGURE 8 Left: Absorption spectra of the glass series A doped with 0.3 mol% Dy^{3+}. Right: Excitation spectra of the same glasses monitored at 572 nm

of the glasses are very similar, with the most intense band at ≈1270 nm which is assigned to the $^6H_{15/2} \rightarrow {}^6F_{11/2}$ transition.[32] This transition is hypersensitive, that is, very sensitive to the host environment.

Figure 8 right shows the excitation spectra of the glasses doped with 0.3 mol% Dy_2O_3 and monitoring the emission at 572 nm. The spectra contain nine bands of which the most intense peak centered at 348 nm is assigned to the $^6H_{15/2} \rightarrow {}^6P_{7/2}$

transition. The peak positions are constant for different Dy^{3+} doping concentrations (the spectra of the glasses doped with 0.1 mol% Dy_2O_3 are not shown here) and the intensities increase with increasing Dy^{3+} content.

The emission spectra of the BP glasses doped with 0.1 and 0.3 mol% Dy_2O_3 under an excitation wavelength of 348 nm are presented in Figure 9. All glasses show a strong emission at ≈571 nm which corresponds to the $^4F_{9/2} \rightarrow {}^6H_{13/2}$ transition.

Three weaker emissions are centered around ≈480, 662, and 753 nm and can be assigned to the $^4F_{9/2}\rightarrow{}^6H_{15/2}$, $^4F_{9/2}\rightarrow{}^6H_{11/2}$, and $^4F_{9/2}\rightarrow{}^6H_{9/2}$ transitions.[33,34] The emission intensity of the most intense peak is highest for the Sr^{2+} and Ca^{2+} containing glass and smallest for the Ba^{2+} glass. The emission intensities increase with increasing Dy^{3+} content, although there is no linear trend, most likely due to concentration quenching, that is also reflected in the decreased lifetime values observed for glasses with a different modifier cation. The hypersensitive $^4F_{9/2}\rightarrow{}^6H_{13/2}$ transition is also an indicator for the Dy^{3+} environment in the host matrix, for example, in a highly symmetric environment the emission intensity will be weaker compared to a distorted one.

The fluorescence decay curves corresponding to the $^4F_{9/2}\rightarrow{}^6H_{13/2}$ and the $^4F_{9/2}\rightarrow{}^6H_{15/2}$ transition (not shown here) were fitted with the bi-exponential function

$$I = I_0 + A_1 exp\left(\frac{t}{\tau_1}\right) + A_2 exp\left(\frac{t}{\tau_2}\right) \quad (2)$$

where τ_1 and τ_2 are the luminescence lifetimes with the respective weighing parameters A_1 and A_2. The average lifetime (τ_{av}) is calculated by using the equation

$$\tau_{av} = \frac{A_1 \cdot \tau_1^2 + A_2 \cdot \tau_2^2}{A_1 \cdot \tau_1 + A_2 \cdot \tau_2} \quad (3)$$
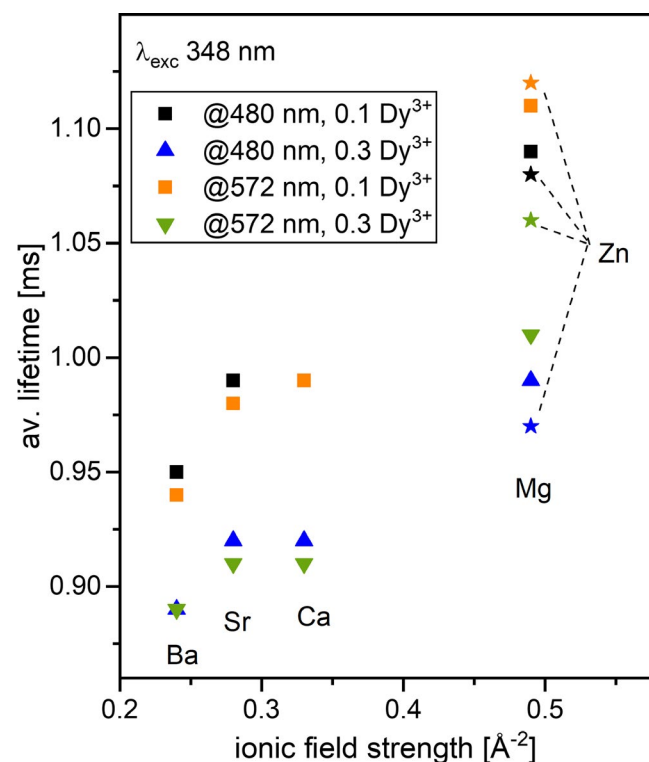

FIGURE 10 Average lifetimes of the 480 nm and 572 nm emission of the glass series A excited at 348 nm

Figure 10 presents the average lifetime of the $^4F_{9/2}$ state for the glasses doped with 0.1 and 0.3 mol% Dy_2O_3 as a function of the respective cation field strength, varying from 0.89 ms to 1.09 ms. Considering the AE-containing glasses, the lifetime increases with an increasing field strength and the glasses doped with 0.1 mol% exhibit a longer lifetime for both emissions. Additionally, the lifetime of the 480 nm emission is higher than the 572 nm emission lifetime in the glasses containing Ba^{2+}, Sr^{2+}, or Ca^{2+}. This trend flips when the high field strength ions are present. Lakshminarayana et al. reported an experimental lifetime of 0.21 ms in a glass with the mol% composition $59.5B_2O_3$-$10WO_3$-$10ZnO$-$10Li_2O$-$10Na_2O$-$0.5Dy_2O_3$,[16] whereas a lifetime of 0.73 ms in a glass with the mol% composition $25BaO$-$5B_2O_3$-$68.8P_2O_5$-$0.2Dy_2O_3$ was measured.[17] The lifetime and weighing factors of the 480 and 572 nm emission are summarized in Table 2 and Table 3.

3.2 | Glass series B: $40ZnO$-xB_2O_3-$(60-x)P_2O_5 + 0.1Dy_2O_3$ with $x = 0, 5, 10$, or 15 mol%

3.2.1 | Glass properties

The compositional dependency of T_g, density, and molar volume of the glass series $40ZnO$-xB_2O_3-$(60-x)P_2O_5$ is presented in Figure 11. The T_g increases with increasing B content from 430°C for 0 mol% B_2O_3 to 532°C for 10 mol% B_2O_3, and remains almost constant when the B content is increased further. The density shows a minimum at a B content of 5 mol%, and then increases almost linearly up to a B content of 15 mol%. The molar volume decreases when

TABLE 2 Fitting parameters of the lifetime measurements under 348 nm excitation and 572 nm emission: $\tau_{1,2}$ lifetime, τ_{exp} the average lifetime, and $A_{1,2}$ the respective weighing factors

Sample	τ_1 [ms]	τ_2 [ms]	τ_{av} [ms]	A_1	A_2
MgBP_01	0.57	1.28	1.11	0.4116	0.5910
MgBP_03	0.51	1.18	1.01	0.4431	0.5593
CaBP_01	0.48	1.08	0.99	0.3001	0.7014
CaBP_03	0.39	3.98	0.91	0.2585	0.7419
SrBP_01	0.58	1.10	0.98	0.3678	0.6335
SrBP_03	0.48	1.01	0.91	0.3125	0.6882
BaBP_01	0.51	1.03	0.94	0.2938	0.7067
BaBP_03	0.56	1.05	0.89	0.4635	0.5371
ZnBP_01	0.64	1.31	1.12	0.4543	0.5486
ZnBP_03	0.67	1.38	1.06	0.6313	0.3710
ZnP_01	0.96	0.32	0.93	0.9273	0.1358
Zn5B55P_01	0.99	0.41	0.94	0.8867	0.1765
Zn15B45P_01	1.11	0.42	1.04	0.8371	0.2235

increasing the B content from ≈41.9 to ≈37.5 cm^3/mol which indicates an enhanced packing density of the coordination polyhedral in the glass network.

3.2.2 | Structural analysis

The Raman spectra of the Zn-containing BP glasses are presented in Figure 12. The spectrum of the pure Zn phosphate glass ($x = 0$) is dominated by two bands: the sharp band at ≈1205 cm^{-1} is assigned to the symmetric stretching vibrations of the phosphate Q^2 groups ($\nu_s(PO_2)$) and the broad band at ≈ 697 cm^{-1} is assigned to the symmetric stretching vibration of the oxygen ion connecting two

TABLE 3 Fitting parameters of the lifetime measurements under 348 nm excitation and 480 nm emission: $\tau_{1,2}$ lifetime, τ_{exp} the average lifetime, and $A_{1,2}$ the respective weighing factors

Sample	τ_1 [ms]	τ_2 [ms]	τ_{av} [ms]	A_1	A_2
MgBP_01	0.60	1.24	1.08	0.4022	0.6001
MgBP_03	0.47	1.10	0.99	0.3208	0.6803
CaBP_01	0.52	1.09	0.99	0.3083	0.6931
CaBP_03	0.45	1.01	0.92	0.2869	0.7134
SrBP_01	0.52	1.09	0.99	0.3084	0.6931
SrBP_03	0.56	1.04	0.92	0.3788	0.6221
BaBP_01	0.47	1.06	0.95	0.2133	0.787
BaBP_03	0.48	0.97	0.89	0.2967	0.7038
ZnBP_01	0.70	1.33	1.09	0.5382	0.4652
ZnBP_03	0.41	1.06	0.97	0.2797	0.7210
ZnP_01	1.00	0.44	0.94	0.8556	0.2124
Zn5B55P_01	0.98	0.34	0.94	0.9160	0.1543
Zn15B45P_01	1.05	0.26	1.02	0.9111	0.1524

phosphate tetrahedral, ($\nu_s(P-O-P)$). Two minor features occur at ≈337 and ≈1271 cm^{-1} and can be assigned to bending vibrations of the phosphate lattice and the symmetric stretching vibration of P = O in phosphate Q^3 units, respectively.[8,9] When boron is introduced into the glass network, the most intense band becomes broader and its maximum shifts to lower wavenumbers, from 1205 to 1190 cm^{-1}. Hudgens et al. discuss the bands at ≈1190 cm^{-1} and 1330 cm^{-1} as "strained" variants of the $\nu_s(PO_2)$ and the $\nu_{as}(PO_2)$.[35] The broad envelop from about 625 to 850 cm^{-1}, assigned to $\nu_s(P-O-P)$, develops sharper features at ≈ 615 and ≈ 770 cm^{-1} which may be associated with stretching vibrations of P-O-B units[4] and the breathing of borophosphate rings.[8] As observed in Figure 12, the gradual replacement of P_2O_5 by B_2O_3 causes, besides broadening, the downshift of $\nu_s(PO_2)$ from 1205 to 1190 cm^{-1} and the upshift of the $\nu_s(P-O-P)$ envelop from 697 to 725 cm^{-1}. These effects are all consistent with an increase in the degree of modification of the phosphate network from $x = 0$ to $x = 15$, that is, toward pyrophosphate units.[25]

The ^{31}P MAS-NMR spectra of the glass series B are presented in Figure 13. All spectra show one signal between −10 and −60 ppm which shifts to higher ppm and becomes broader as the B content increases, that is, from −34.3 ppm ($x = 0$) to −30.4 ($x = 15$). This was also reported by Doumert et al. for a similar set of Zn^{2+}-containing BP glasses.[31] With additional 2D NMR experiments, they could show that the phosphate and tetrahedral borate units mix even at low B contents and form B-O-P links.[31] As observed in the Raman spectra and discussed above, the substitution of P by B (5 < x < 15 mol%) leads to a depolymerization of the phosphate network which results in an increase in Q^1, whereas the amounts of Q^2 and Q^3 should decrease. The variety of possible B-O-P links and the complexity of the NMR spectra does not allow a reliable deconvolution of the spectra at this point, and advanced NMR experiments should be performed.

FIGURE 11 T_g, density, and molar volume of the glass series B, $40ZnO-xB_2O_3-(60-x)P_2O_5$
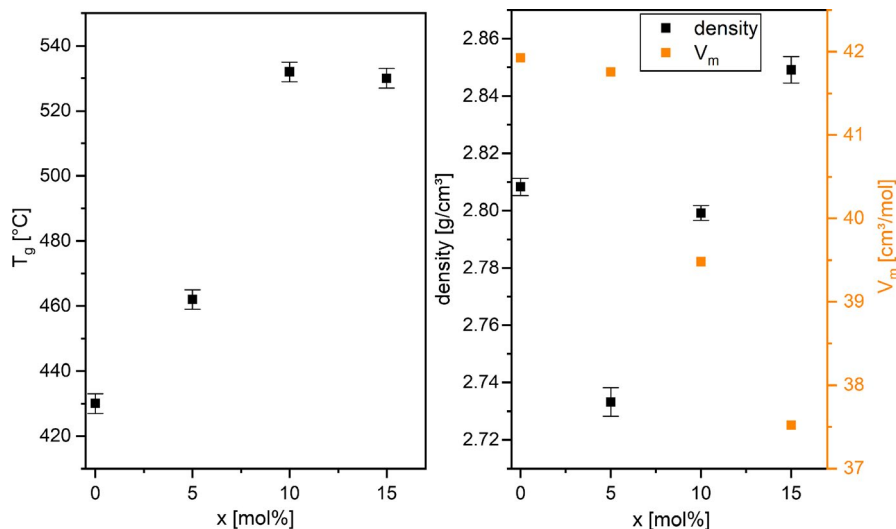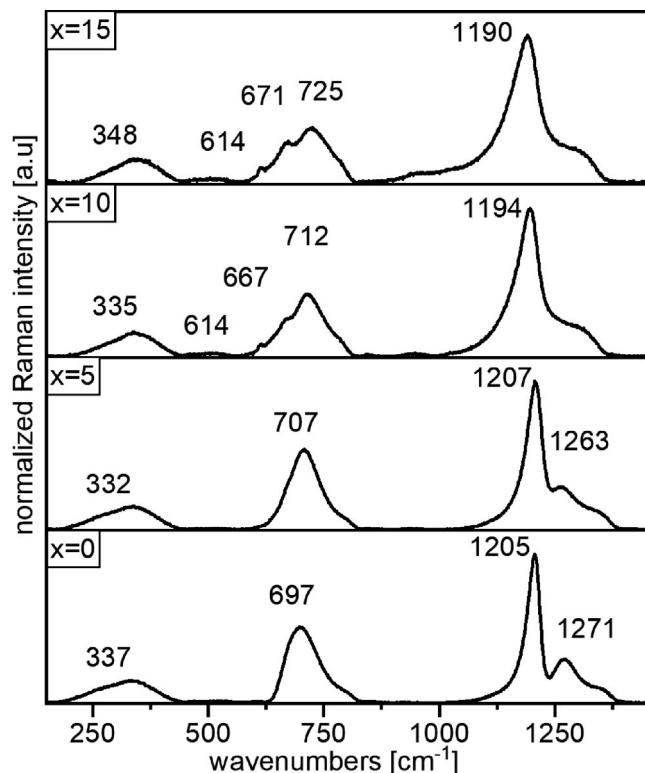
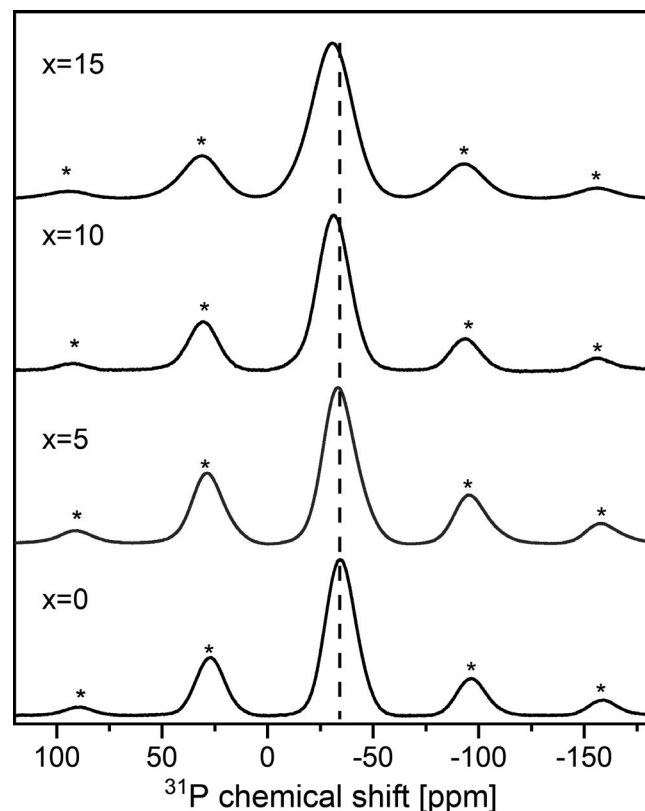**FIGURE 12** Normalized Raman spectra of the glass series B recorded at 633 nm

FIGURE 13 ^{31}P MAS-NMR spectra of the glass series B. The spinning side bands are marked with asterisks

3.2.3 | Luminescence properties

The emission spectra of the glass series B excited using 348 nm are presented in Figure 14. The spectra show the typical four emission bands already discussed above. The intensities of all these bands decrease with increasing x.

Decreasing the PO_4 content while simultaneously increasing the BO_4 content leads to an increase in the ionic character of the glass. This, and a more symmetric local Dy^{3+} ion environment, cause the decrease in the emission intensity.[36] The average lifetime of the 483 and 572 nm emission as a function of the B content is presented in Figure 15. The 572 nm lifetime increases from 0.93 (x = 0) to 1.13 ms (x = 10) and then decreases again to 1.04 ms. The 483 nm lifetime follows the same trend with similar or slightly lower values.
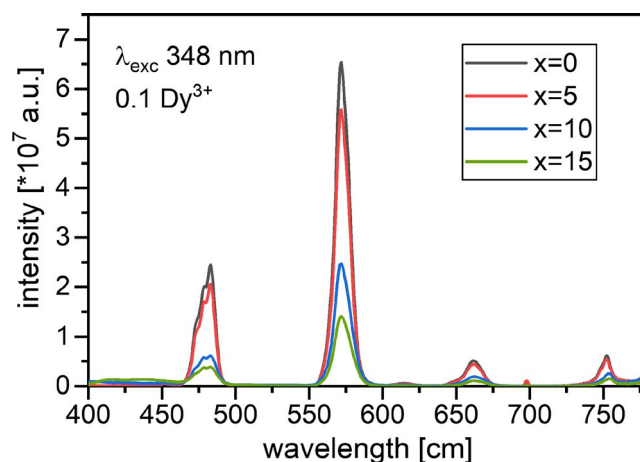

FIGURE 14 Emission spectra excited at 348 nm of the glass series B doped with 0.1 mol% Dy_2O_3
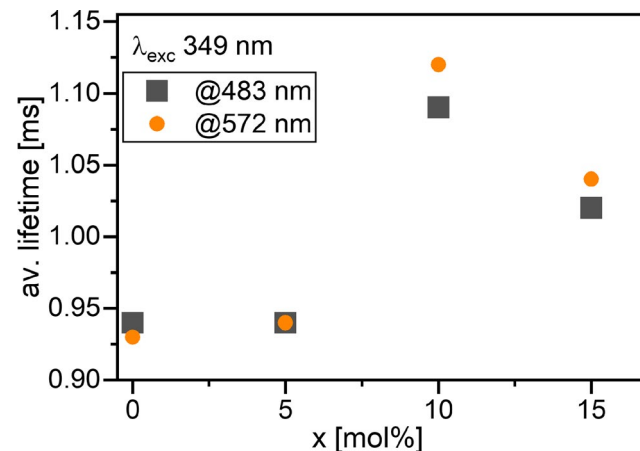

FIGURE 15 The average lifetime of the 483 and 572 nm emission of glass series B

4 | DISCUSSION

Varying the divalent cation in glass series *A* causes several changes in their structure and properties. Figure 1 and Table 1 show that the T_g values increase with an increasing cation field strength within the AE cation series, due to the reduced mobility of the BP glass network and the stronger M-O interactions. The density and molar volume increase with an increasing cation radius. Exceptions are the Mg^{2+} and Zn^{2+} glasses, which show the same and comparably high molar volume of 39.48 cm^3/mol, indicating a more constrained glass structure, as the displacement of the basic structure is limited.

The Raman and FTIR spectra are very similar when varying the cation and the absence of BO_3 is noted. This is also confirmed by the ^{11}B NMR spectra, which show that the boron atoms occur only in fourfold configuration (BO_4). The ^{31}P NMR spectra contain one broad signal which shifts to higher fields with increasing field strength as the Q^i units become more shielded. Although a detailed deconvolution of the spectra is not possible at the moment, some qualitative statements can be made. In the right part of Figure 5, a broadening of the main signal is discernible from Ba^{2+} to Zn^{2+}. Previous studies on AE containing metaphosphate glasses observed an increase in the Q^2 and Q^3 bandwidths with an increasing cation field strength.[24] This reflects more variations of P-O bond angles and bond lengths,[37–40] and the introduction of B increases further the possible variations. Stronger M-O interactions between the high field strength Mg^{2+}/Zn^{2+} cations and the non-bridging oxygens of the Q^i units cause distortions in the PO_4 environments. As the M-O bond is much more localized, a structural adaption in its nearest vicinity is required.[24] These structural variations could cause the increased molar volume of these glasses, as well as the larger amounts of Q^3 which will occupy a larger volume.

The emission spectra of the glasses with varying divalent cations are similar. The two strongest emissions assigned to the $^4F_{9/2} \rightarrow ^6H_{13/2}$ (yellow) and $^4F_{9/2} \rightarrow ^6H_{15/2}$ (blue) transition, are electric dipole and magnetic dipole transitions, respectively. The intensity ratio of these transitions can be used as a measure for the symmetry of the Dy^{3+} local environment.[41] Ratio values <1 indicate a glass matrix with comparably high local symmetry around the Dy^{3+} ion.[42–45]

The transition ratios of the glasses with varying cations are presented in Figure 16. An almost linear increase in the ratio with the increasing ionic field strength is discernible for both Dy^{3+} doping concentrations. The ratio of the Mg^{2+} containing glass doped with 0.1 mol% Dy_2O_3 is about 50% higher than for the doping concentration of 0.3 mol%. The trend of the transition ratios is in perfect agreement with the previous results: The Mg^{2+} and Zn^{2+} containing glasses show more local variations in their glass structure due to the strong M-O bond. This is reflected in the molar volume,
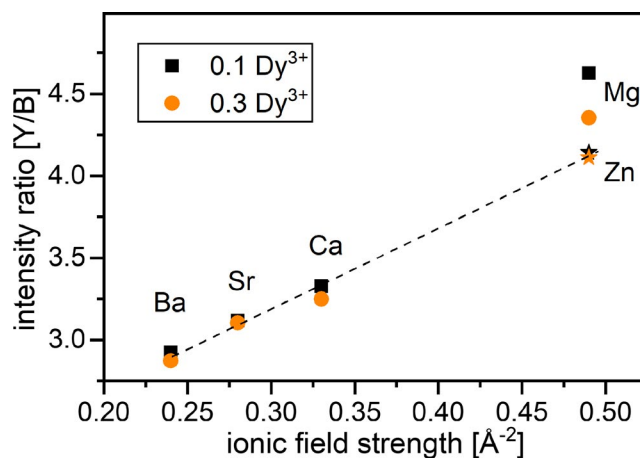

FIGURE 16 The intensity ratio of the $^4F_{9/2} \rightarrow ^6H_{13/2}$ (yellow) and $^4F_{9/2} \rightarrow ^6H_{15/2}$ (blue) transitions of both Dy^{3+} doping concentrations as a function of the cation field strength in glass series A. The line is drawn to guide the eye
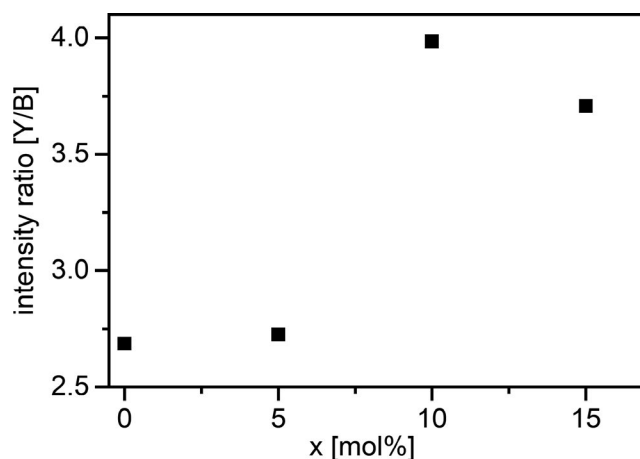

FIGURE 17 The intensity ratio of the $^4F_{9/2} \rightarrow ^6H_{13/2}$ (yellow) and $^4F_{9/2} \rightarrow ^6H_{15/2}$ (blue) transitions of the glass series B as a function of B_2O_3 content, x

the vibrational and NMR spectra and consequently in their emission spectra and fluorescence lifetime presented in Figure 8.

Following the above argument, it has to be assumed that the structural variations around Dy^{3+} ions are lower in the glass series *B* with x < 10 mol% (see Figure 17), mainly because not enough borate units are present. As x is further increased, the structural variety decreases again which is reflected in the Raman and ^{31}P NMR spectra (see Figure 12 and Figure 13). This may be linked to the formation of B-O-B structural units and results in a lower lifetime. Nevertheless, it has to be noted that the molar volume as well as the emission intensities in the second series of BP glasses are the highest for x≤ 10.

5 | SUMMARY AND CONCLUSIONS

This study provides a systematic investigation on the influence of different divalent cations (M) and of the boron to phosphorous ratio (B/P) on the emission properties of Dy^{3+} ions in two series of borophosphate glasses. Thermal and physical properties such as T_g, ρ, and V_m were determined and show a strong dependence on the ionic field strength of the cation. Raman, FTIR, and NMR spectroscopic measurements show an increased variety of structural units, for example, increasing bandwidths, with increasing cation field strength and with increasing B content up to 10 mol% B_2O_3. The variety of structural units and the rearrangement of the BP network, caused by the strong M-O interactions, create a local Dy^{3+} environment with comparably low symmetry which results in a longer emission lifetime.

ORCID

Kristin Griebenow https://orcid.org/0000-0001-9583-4478
Francisco Muñoz https://orcid.org/0000-0002-7322-6559
Nagia S. Tagiara https://orcid.org/0000-0002-1347-8287
Róbert Klement https://orcid.org/0000-0001-5935-8312
Anna Prnová https://orcid.org/0000-0002-1713-3171
Bruno Wolfrum https://orcid.org/0000-0001-9818-8811
Efstratios I. Kamitsos https://orcid.org/0000-0003-4667-2374
Alicia Duran https://orcid.org/0000-0002-0067-1934
Dušan Galusek https://orcid.org/0000-0001-5995-8780

REFERENCES

1. Reddy CM, Prasad Raju BD, Sushma NJ, Dhoble NS, Dhoble SJ. A review on optical and photoluminescence studies of Re^{3+} ions doped LCZSFB glasses. Renew Sustain Energy Rev. 2015;51:566–84.
2. Brow R. Review: The structure of simple phosphate glasses. J Non-Cryst Solids. 2000;263&264:1–28.
3. Yiannopoulos YD, Chryssikos GD, Kamitsos EI. Structure and properties of alkaline earth borate glasses. Phys Chem Glasses. 2001;42:164–72.
4. Christensen R, Olson G, Martin SW. Structural studies of mixed glass former gasses by Raman and ^{11}B and ^{31}P magic angle spinning nuclear magnetic resonance spectroscopies. J Phys Chem B. 2013;117:2169–79.
5. Hermansen C, Youngman RE, Wang J, Yue Y. Structural and topological aspects of borophosphate glasses and their relation to physical properties. J Chem Phys. 2015;142:184503.
6. Takebe H, Harada T, Kuwabra M. Effect of B_2O_3 addition on the thermal properties and density of barium phosphate glasses. J Non-Cryst Solids. 2006;352:709–13.
7. Ducel JF, Videau JJ. Physical and chemical characterization of sodium borophosphate glasses. Mater Lett. 1992;13:271–4.
8. Anastasopoulou M, Vasilopoulos KC, Anagnostopoulos D, Koutselas I, Papayannis DK, Karakassides MA. Structural and theoretical study of strontium borophosphate glasses using Raman Spectroscopy and Ab initio molecular orbital method. J Phys Chem B. 2017;121:4610–9.
9. Koudelka L, Mosner P. Borophosphate glasses of the $ZnO-B_2O_3$-P_2O_5 system. Mater Lett. 2000;42:194–9.
10. Koudelka L, Kalenda P, Mosner P, Cernosek Z, Montagne L, Revel B. Structural investigation of $BaO-B_2O_3-P_2O_5$ glasses by NMR and Raman spectroscopy. J Mol Structure. 2016;1119:212–9.
11. Kalenda P, Koudelka L, Mosner P, Benes L. Thermal behaviour and the properties of $BaO-B_2O_3-P_2O_5$ glasses. J Therm Anal Calorim. 2016;124:1161–8.
12. Kim YS, Choi WG, Ryu BK. Effect of ZnO content change on the structure and properties of zinc borophosphate glasses. Glass Phys Chem. 2014;40:408–14.
13. Chen P, Li S, Qiao W, Li Y. Structure and crystallization of $ZnO-B_2O_3-P_2O_5$ glasses. Glass Phys Chem. 2011;37:29–33.
14. Kiran N, Kumar AS. White light mission from Dy doped sodium lead borophosphate glasses under UV light excitation. J Mol Structure. 2013;1054–1055:6–11.
15. Jayasimhadri M, Jang K, Lee HS, Chen B, Yi SS, Jeong JH. White light generation from Dy doped Zn borophosphate glasses. J Appl Phys. 2009;106:013105.
16. Chanthima N, Tariwong Y, Kiwsakunkran N, Kaewkhao J. Effects of BaO and Bi_2O_3 on the optical and luminescence properties of Dy^{3+} doped borophosphate glasses. J Phys Conf Series. 2019;1259:012003.
17. Karki S, Kesavulu CR, Kim HJ, Kaewkhao J, Chanthima N, Kothan S, et al. Physical, optical and luminescence properties of the Dy^{3+} doped barium borophosphate glasses. J Non-Cryst Solids. 2019;521:119483.
18. Seshadri M, Radha M, Bell MJV, Anjos V. Structural and spectroscopic properties of Yb doped borophosphate glasses for IR laser application. Ceram Int. 2018;44:20790–7.
19. Naseer KA, Marimuthu K. The impact of Er/Yb co-doping on the spectroscopic performance of Bi borophosphate glasses for photonic applications. Vacuum. 2021;183:109788.
20. Vijayakumar M, Marimuthu K, Sudarsan V. Concentration dependent spectroscopic behaviour of Sm doped leadfluoro borophosphate glasses for laser and Led applications. J Alloys Comp. 2015;647:209–20.
21. Kamitsos EI, Patsis AP, Karakassides MA, Chryssikos GD. Infrared reflectance spectra of lithium borate glasses. J Non-Cryst Solids. 1990;126:52–67.
22. Dietzel VA. Die Kationenfeldstärke und ihre Beziehungen zu Entglasungsvorgängen, zur Verbindungsbildung und zu den Schmelzpunkten von Silicaten. Ztschr Elektrochem. 1942;48:9.

23. Griebenow K, Kamitsos EI, Wondraczek L. Mixed-modifier effect in (Ca, Mg) metaphosphate glasses. J Non-Cryst Solids. 2017;468:74–81.

24. Griebenow K, Bragatto CB, Kamitsos EI, Wondraczek L. Mixed-modifier effect in alkaline earth metaphosphate glasses. J Non-Cryst Solids. 2018;481:447–56.

25. Palles D, Konidakis I, Varsamis CPE, Kamitsos EI. Vibrational spectroscopic and bond valence study of structure and bonding in Al_2O_3-containing AgI-$AgPO_3$ glasses. RSC Adv. 2016;6:16697–710.

26. Tagiara NS, Palles D, Simandrias ED, Psycharis V, Kyritsis A, Kamitsos EI. Synthesis, thermal and structural properties of pure TeO_2 glass and zinc tellurite glasses. J Non-Cryst Solids. 2017;457:116–25.

27. Velli LL, Varsamis CPE, Kamitsos EI, Möncke D, Ehrt D. Structural Investigation of metaphosphate glasses. Phys Chem Glasses. 2005;46:178–18.

28. Yao ZY, Möncke D, Kamitsos EI, Houizot P, Celarie F, Rouxel T, et al. Structure and mechanical properties of copper-lead and copper-zinc borate glasses. J Non-Cryst Solids. 2016;435:55–68.

29. Möncke D, Palles D, Zacharias N, Kaparou M, Kamitsos EI, Wondraczek L. Formation of an outer borosilicate glass layer on Late Bronze Age Mycenaean blue vitreous relief fragments. Phys Chem Glasses: Eur J Glass Sci Technol B. 2013;54:52–9.

30. Massiot D, Fayon F, Capron M, King I, Le Calvé S, Alonso B, et al. Modelling one- and two-dimensional solid-state NMR spectra. Magn Res Chem. 2002;40:70–6.

31. Doumert B, Lecomte F, Tricot G. Advanced solid state 1D/2D NMR investigation of the B_2O_3 $Zn(PO_3)_2$ glasses. J Non-Cryst Solids. 2020;548:120325.

32. Carnall WT, Fields PR, Rajnak K. Electronic energy levels in the trivalent lanthanide Aquo Ions. J Chem Phys. 1968;49:4424.

33. Lakshminarayana G, Baki SO, Lira A, Kityk IV, Caldino U, Kaky KM, et al. Structural, thermal and optical investigations o Dy^{3+} doped B_2O_3-WO_3-ZnO-Li_2O-Na_2O glasses for warm white light emitting applications. J Lum. 2017;186:283–300.

34. Shoaib M, Rajaramakrishna R, Rooh G, Chanthima N, Kim HJ, Saiyasombat C, et al. Structural and luminescence study of Dy^{3+} doped phosphate glasses for solid state lighting applications. Opt Mater. 2020;109:110322.

35. Hudgens JJ, Brow RK, Tallant DR, Martin SW. Raman spectroscopy study of the structure of lithium and sodium ultraphosphate glasses. J Non-Cryst Solids. 1998;223:21–31.

36. Vijayakumar M, Marimuthu K. Structural and luminescence properties of Dy doped oxyfluoro-borophosphate glasses for lasing materials and white LEDs. J Alloys Compounds. 2015;629:230–41.

37. Brow RK, Phifer CC, Turner GL. Cation effects on ^{31}P MAS NMR chemical shifts of metaphosphate glasses. J Am Ceram Soc. 1991;74:1287–90.

38. Feike M, Jäger C, Spiess HW. Connectivities of coordination polyhedral in phosphate glasses from ^{31}P double-quantum NMR spectroscopy. J Non-Cryst Solids. 1998;223:200–6.

39. Witter R, Hartmann P, Vogel J, Jäger C. Measurements of chain length distributions in calcium phosphate glasses using 2D ^{31}P double quantum NMR. Solid State Nucl Magn Reson. 1998;13:189–200.

40. Fayon F, Bessada C, Coutures JP, Massiot D. High-Resolution Double-Quantum ^{31}P MAS NMR study of the intermediate-range order in crystalline and glass lead phosphates. Inorg Chem. 1999;38:5212–8.

41. Tanabe S, Kang J, Hanada T, Soga N. Yellow/blue luminescence of Dy^{3+} doped borate glasses and their anomalous temperature variations. J Non-Cryst Solids. 1998;239:170–5.

42. Rajesh D, Ratnakaram YC, Seshadri M, Balakrishna A, Krishna TS. Structural and luminescence properties of Dy ion in Sr Li Bi borate glasses. J Lum. 2012;132:841–9.

43. Linganna K, Srinivasa Rao RC, Jayasankar CK. Optical properties and generation of white light in Dy^{3+} doped lead phosphate glasses. J Quant Spect Radiat Trans. 2013;118:40–8.

44. Vijayakumar M, Jamalaiah BC, Rama K, Reddy RR. Optical absorption and fluorescence studies of Dy^{3+} doped lead telluborate glasses. J Lum. 2012;132:86–90.

45. Sureshkumar J, Pavani K, Mohan B, Giri K, Rai SB, Moorthy LR. Fluorescence characteristics of Dy^{3+} ions in calcium fluoroborate glasses. J Lum. 2010;130:1916–23.